Scripta Materialia 146 (2018) 31–35

Contents lists available at ScienceDirect

Scripta Materialia

journal homepage: www.elsevier.com/locate/scriptamat

Regular article

# Towards a realistic prediction of sintering of solid oxide fuel cell electrodes: From tomography to discrete element and kinetic Monte Carlo simulations

Z. Yan [a,*], S. Hara [b], N. Shikazono [a]

[a] Institute of Industrial Sciences, The University of Tokyo, Komaba 4-6-1, Meguro-ku, Tokyo 153-8505, Japan
[b] Department of Mechanical Engineering, Faculty of Engineering, Chiba Institute of Technology, Tsudanuma 2-17-1, Narashino, Chiba 275-0016, Japan

ARTICLE INFO

*Article history:*
Received 3 September 2017
Received in revised form 30 October 2017
Accepted 30 October 2017
Available online xxxx

*Keywords:*
Sintering
Discrete element method
Kinetic Monte Carlo
Microstructure evolution
Solid oxide fuel cells

ABSTRACT

The 3-dimensional (3D) particle geometries in sub-micrometric $La_{0.6}Sr_{0.4}Co_{0.2}Fe_{0.8}O_{3-\delta}$ powder are obtained by high-resolution focused ion beam scanning electron microscope (FIB-SEM) tomography. Irregularly shaped particles are represented with volume equivalent single spheres (single-sphere model) or clumped multispheres (multi-sphere model), based on their 3D geometries. The discrete element method (DEM) is used to reproduce "virtual" powder packings with multi-sphere and single-sphere models. The DEM-generated virtual microstructures and the FIB-SEM real microstructures are submitted to kinetic Monte Carlo (KMC) simulations of sintering. It is shown that the multi-sphere model predicts more realistic microstructure than the single-sphere model for sintering of $La_{0.6}Sr_{0.4}Co_{0.2}Fe_{0.8}O_{3-\delta}$.



Solid oxide fuel cells (SOFCs) are promising energy conversion devices for their excellent energy efficiency and fuel flexibility. Microstructural characteristics such as triple phase boundary length, specific surface area and tortuosity factors of different phases in electrodes strongly affect the electrochemical reaction and ion/electron/gas conductions, and finally the performance of SOFCs. Sintering phenomenon during the fabrication and the long-term operation at elevated temperature plays an important role in the microstructural evolutions of SOFC electrodes. In recent years, 3-dimensional (3D) characterizations in X-ray computed tomography (CT) [1] and focused ion beam scanning electron microscope (FIB-SEM) tomography [2] have enabled 3D characterizations of the microstructures in SOFC electrodes.

Accordingly, a number of numerical models have been used to investigate the microstructural changes in the SOFC electrodes during sintering. The molecular dynamic (MD) method can model the sintering of several tens or hundreds of nanoparticles [3–5]. The discrete element method (DEM) method has been used to model sintering of metals [6], ceramics [7], and metal/ceramic composites [8], and therefore it has great potential of modeling SOFC electrodes [9]. However, grain coarsening is still challenging for DEM simulations of sintering. The phase field method (PFM) is also used to model the microstructural evolution of SOFC electrodes [10–12]. When microstructure feature size is smaller than the diffuse-interface thickness, the PFM method may produce some artifacts [13]. The Potts kinetic Monte Carlo (KMC) method is recently emerging as a mesoscale tool to mimic microstructure change during sintering [14–16]. Hara et al. [17–19] and Zhang et al. [20,21] modeled the microstructural evolutions of various SOFC electrode materials in KMC simulations. Most KMC simulations of sintering either treat the initial microstructure as packing of spheres [15,16,20,22,23] or use the real microstructure obtained by X-ray CT [14] or FIB-SEM tomography [17,19]. The former one with spherical particles which neglect the realistic local curvature and particle interaction will lead to unrealistic prediction. Yan et al. [24] showed that the powder morphology had a strong effect on sintering kinetics and microstructures. On the other hand, the latter requires the use of X-ray CT or FIB-SEM which is expensive and time-consuming. In this context, we report a novel numerical scheme to reproduce realistic microstructures for KMC simulations of sintering of SOFC electrodes starting from modeling of real powders.

A commercial $La_{0.6}Sr_{0.4}Co_{0.2}Fe_{0.8}O_{3-\delta}$ (LSCF) cathode powder (fuelcellmaterials Inc., USA) with a nominal diameter size of $D_{50} = 1.0$ μm was reconstructed with FIB-SEM tomography (cf. Ref. [19] for details), and a volume of 997 × 466 × 320 voxels (voxel size 25 × 25 × 25 $nm^3$) was obtained (Fig. 1(a)). The marker-based 3D watershed segmentation module in Avizo Fire 8.1 (FEI VSG, Merignac, France) was used to segment the particles, resulting in ~11,000 particles (Fig. 1(b)). Particles' volumes ($V$) and surface areas ($A$) were calculated using the label analysis module in Avizo. The volume equivalent particle size ($D_V$) is calculated as $D_V = (6V/\pi)^{1/3}$ and sphericity ($\Phi$) is calculated

* Corresponding author.
*E-mail addresses:* zilin@iis.u-tokyo.ac.jp, zilinyan@gmail.com (Z. Yan).

https://doi.org/10.1016/j.scriptamat.2017.10.035
1359-6462/

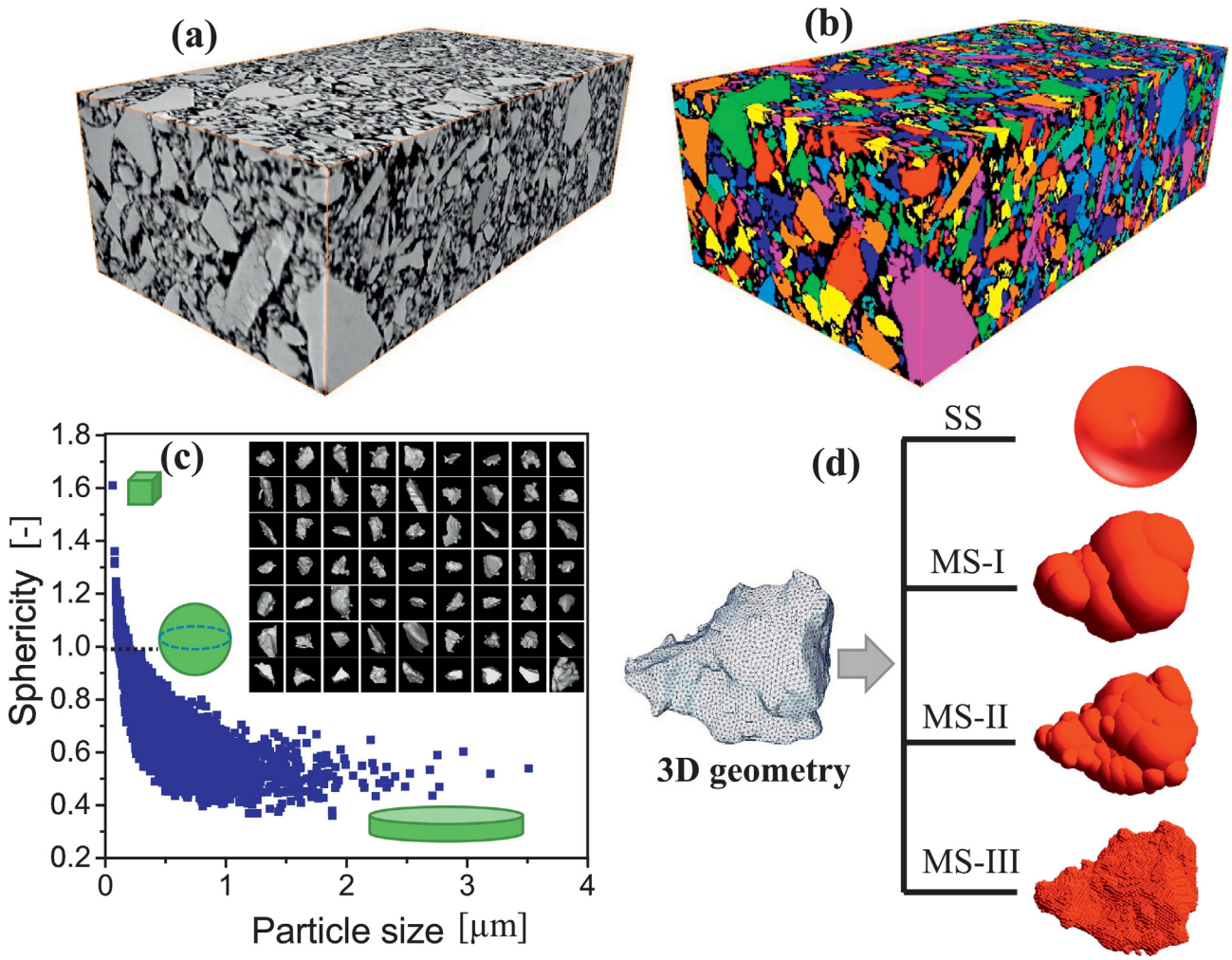


**Fig. 1.** (a) FIB-SEM 3D reconstruction of press packed LSCF raw powders; (b) marker-controlled watershed segmentation of particles; (c) particle sphericity distribution and the inset figure shows some typical particle shapes; (d) real particle represented using multispheres.

as $\Phi = \pi^{1/3}(6V)^{2/3}/A$. Particles with $\Phi$ values close to 1.0 are almost spherical. The particle sphericity distribution in Fig. 1(c) shows that fine particles and most small particles ($D \leq 500$ nm) have high sphericity values while some large particles appear to have a plate-like shape with very low sphericity values (about 0.4). Thus, assuming all the particles as spheres will ignore the plate-like feature of these large particles.

To consider the realistic shapes of particles, we use a multi-sphere method [25] to approximate irregularly shaped particles by conjoining multiple spheres as one rigid body following a multisphere tree algorithm [26]. Four different approximation levels are considered as shown in Fig. 1(d). The single-sphere (SS) model assumes each particle as a volume equivalent sphere. The multi-sphere (MS) model includes a low-level (MS-I) approximation using 8 overlapping spheres and a high-level (MS-II) approximation using 64 overlapping spheres. A non-overlapping multi-sphere model (MS-III) is also used to represent the particles by replacing each voxel of the particle with an inscribed sphere. For the MS-III model, density of each sphere is multiplied by a factor of $6/\pi$ so that the total mass is conserved.

Four powder packings (see Table 1) with different approximation levels were modeled in DEM using an open-source code LIGGGHTS® [25]. The DEM models are detailed in Ref. [24]. Sample SS treated all the particles with SS model. Sample MS-I treated fine particles ($D \leq 200$ nm) with SS model and the rest with MS-I model. Sample MS-II treated fine particles ($D \leq 200$ nm) with SS model, medium-sized particles ($200 < D \leq 500$ nm) with MS-I model and large ones ($D > 500$ nm) with MS-II model. This treatment is to speed up the DEM computation by avoid using too small and too many spheres in the clumps for fine particles, which require a very small time step for the DEM simulations. Actually, according to the statistics of sphericity of the real particles (Fig. 1(c)), the fine particles have very high sphericity values. In a sintering point of view, fine particles are highly thermodynamically unstable and turn into spheres rapidly by sintering. Therefore, it is reasonable

**Table 1**
Details for the numerical samples in this study. The number of spheres in the four realizations of the MS-III model varies in the range of 2–3 millions. The number of spheres in the table for sample MS-III is just one example.

| Samples | Approximation models | Density/[kg/m$^3$] | Number of spheres |
|---|---|---|---|
| Sample SS | SS: all size range | 6,360 | 10,880 |
| Sample MS-I | SS: <200 nm; MS-I: ≥200 nm | 6,360 | 70,184 |
| Sample MS-II | SS: <200 nm; MS-I: 200–500 nm; MS-II: ≥500 nm | 6,360 | 134,650 |
| Sample MS-III | MS-III: all size range | 12,147 | 2,463,260 |